Journal of Fluids and Structures 17 (2003) 793–811

JOURNAL OF FLUIDS AND STRUCTURES

www.elsevier.nl/locate/jnlabr/yjfls

Vortex shedding and fluidelastic instability in a normal square tube array excited by two-phase cross-flow

P.A. Feenstra[a], D.S. Weaver[a,*], T. Nakamura[b]

[a] *Department of Mechanical Engineering, McMaster University, 1280 Main Street West, Hamilton, Ont., Canada L8S 4L7*
[b] *Takasago R&D Center, Mitsubishi Heavy Industries, 2-1-1 Shinhama Aria, Takasago, Hyogo, Japan*

Received 7 March 2002; accepted 3 February 2003

Abstract

Laboratory experiments were conducted to determine the flow-induced vibration (FIV) response and fluidelastic stability threshold of a model heat exchanger tube bundle subjected to a cross-flow of refrigerant 11. The tube bundle consisted of a normal square array of 12 tubes with outer tube diameters of 7.11 mm and a pitch over diameter ratio of 1.485. The experiments were conducted in a flow-loop that was capable of generating single- and two-phase cross-flows over a variety of mass fluxes and void fractions. The primary intent of the research was to improve our understanding of the FIVs of heat exchanger tube arrays subjected to two-phase cross-flow. Of particular concern was the effect of array pattern geometry on fluidelastic instability. The experimental results are analysed and compared with existing data from the literature using various methods of parameter definition. Comparison of tube vibration response in liquid flow with previous results shows a similar occurrence of symmetric vortex shedding that validates the scale model approach in single-phase flow. It was found that the introduction of a small amount of bubbles in the flow disrupted the vortex shedding and thereby caused a significant reduction in streamwise vibration amplitude. The fluidelastic stability thresholds for the present array agree well with results from previous studies. Furthermore, a good collapse of the stability data from various investigations is obtained when the fluid density is defined using the slip model of Feenstra et al. and when an effective two-phase flow velocity is defined using the interfacial velocity model of Nakamura et al.

Keywords: Two-phase flow; Heat exchanger tube array; Flow-induced vibration

1. Introduction

Two-phase flow-induced vibration (FIV) of an array of cylinders is the subject of this paper. The research was designed to shed new light on the FIV that occurs in the U-bend region of a nuclear steam generator by experimenting with a scale model heat exchanger tube array subjected to two-phase R-11 cross-flow. Fluidelastic instability (FEI) is the vibration mechanism of primary interest because it is the most damaging in the short term, and can cause the tubes to vibrate excessively, leading to rapid fatigue or wear at the tube supports. However, periodic excitation by coherent vorticity phenomena and turbulence may also lead to damaging vibrations and, in heavy fluids, may influence the onset of FEI. An overview of FIV in power and process plant components is provided by Weaver et al. (2000).

Most of the early experimental research in the field of FIV in heat exchangers relied on sectional scale models of tube arrays subjected to single-phase fluids such as air or water. Complete reviews on the topic are provided by Païdoussis

*Corresponding author. Tel.: +1-905-525-9140x24907; fax: +1-905-572-7944.
E-mail addresses: feenstpa@mcmaster.ca (P.A. Feenstra), weaverds@mcmaster.ca (D.S. Weaver), nakamura@wj.trdc.mhi.co.jp (T. Nakamura).

0889-9746/03/$ - see front matter
doi:10.1016/S0889-9746(03)00024-0

(1982) and Weaver and Fitzpatrick (1988). More recently, researchers have expanded the study to include two-phase flows, which occur in nuclear steam generators and many other tubular heat exchangers. For an overview of two-phase FIV research, see Pettigrew and Taylor (1994).

The cheapest and simplest approach to perform an experimental study of two-phase excited tube vibration is to model the two-phase flow by mixing air and water at atmospheric pressure. However, air–water flows have a much different density ratio between the phases than steam–water flow and this will affect the difference in flow velocity between the phases. The liquid surface tension, which controls bubble size, is also not accurately modelled in air–water mixtures. For these reasons, it has become more common in recent years to simulate steam flows using refrigerants, which boil at or near atmospheric pressure and temperature conditions. For example, Pettigrew et al. (1995) used refrigerant 22 (R-22) while the present research used an R-11 loop (Feenstra et al., 1995). The use of R-11 as a modelling fluid is a reasonable alternative because it approximates the density ratio, liquid surface tension and liquid viscosity of steam–water mixtures more accurately than air–water mixtures. It also permits local interaction between phases that could affect damping and added fluid mass such as vapour flashing and bubble collapse due to tube motion induced pressure fluctuations. Clearly, air–water mixtures will not simulate these phenomena.

Traditionally, researchers have relied on the homogeneous equilibrium model (HEM) to determine the pertinent fluid parameters in two-phase flow such as density, void fraction and flow velocity. This model treats the two-phase flow as homogeneous in density and temperature with no difference in velocity between the gas and liquid phases. It has been widely used because it is easy to implement and no reliable alternative was generally available. The main drawback with using the HEM is that it assumes a velocity ratio of unity between the gas and liquid phases (i.e., $U_G/U_L = 1$). This assumption is not accurate in the case of vertical upward flow where the density difference between the gas and liquid creates a significant buoyancy or gravity effect. The density ratios for air–water is roughly 830:1 while for steam water it is only about 33:1 so that the velocity ratio (slip ratio) of these two fluids is expected to be quite different. In comparison, the density ratio of R-11 at 40°C is about 150:1. Earlier work by the present authors (Feenstra et al., 1995, 2000a) as well as the present study utilized gamma densitometry to measure the actual void fraction in the test-section, and it was found to be much lower than that predicted by the HEM. This led to the development of a new model by Feenstra et al. (2000b) for predicting the void fraction in upward two-phase flows in horizontal tube bundles. Comparison with other researchers' measurements of void fraction in tube bundles for air–water and R-113, showed remarkably good agreement using this new model.

This paper presents the results of an experimental study of two-phase R-11 cross-flow excited vibrations in a square in-line tube array with a pitch ratio of 1.485. The results for vorticity excitation and FEI are compared with previous results for tube arrays of different geometries and working fluids. Finally, the stability data are analysed using different definitions of two-phase velocity and density in an attempt to improve our scale modelling of FEI in tube arrays.

2. Description of the experiments

2.1. Flow-loop

The flow-loop was specially constructed to produce a uniform velocity and void distribution cross-flow in the test-section, using refrigerant 11 (trichlorofluoromethane, CCl_3F) as the working fluid. The advantage of using this fluid to model the actual steam–water flow in a nuclear steam generator is that R-11 requires roughly 1/13th the amount of enthalpy to generate a vapour. Thus a two-phase flow of R-11 can be generated with greatly reduced heating power and the flow-loop can be operated at a much reduced pressure, thereby reducing the cost of the experiments as compared to a steam–water loop. The fluid is circulated by a gear pump with a practical pumping capacity of 2.2 L/s. Vapour is generated in the heater section (just upstream of the test-section) by electric heating elements which are presently configured for 19.2 kW maximum power. The R-11 flows vertically upward into the test-section, where the model tube bundle is located. For more details on the flow-loop, see Feenstra et al. (1995).

2.2. Test-section and tube bundle

The focal point of the loop is the test-section, where the model tube bundle is mounted. It is a rectangular flow channel with cross-sectional dimensions of 31.75 mm × 305 mm. It is equipped with large side widows for flow visualization and an end window to permit vibration measurement with a nonintrusive optical probe. The test-section and flow-loop are equipped with thermocouples to monitor fluid temperature around the loop for determining the flow quality of the R-11 entering the test-section. A gamma densitometer was used in this study to permit nonintrusive measurement of void fraction of the two-phase flow in the test-section.

The tube bundle consisted of 12 horizontally mounted brass tubes, 7.11 mm in diameter, 305 mm long in a normal square pattern with a pitch over diameter ratio of 1.485. The tubes were cantilever mounted into a solid brass block, and tuned to within $\pm 0.2\%$ of the average in-air natural frequency of 35.5 Hz. More details of the tested tube bundle are given in Table 1 and an illustration of the tube bundle cross-section is given in Fig. 1. The tube vibration response was measured with a special optical light probe, which is described in detail in Judd et al. (1992). The output of this device was processed by a dynamic analyser (model HP35670A), which calculated the r.m.s. amplitude and frequency spectrum in the frequency range from 0 to 100 Hz. The number of sample averages used for determining two-phase response (i.e., amplitude, frequency and damping) was 100, while for single-phase flow tests, only 25 sample averages were sufficient to obtain repeatable results.

2.3. Determination of two-phase flow parameters

A general expression for void fraction, α, in a two-phase flow is given by

$$\alpha = \left[1 + S\frac{\rho_G}{\rho_L}\left(\frac{1}{x} - 1\right)\right]^{-1}, \tag{1}$$

Table 1
Design parameters of experimental tube bundles

Parameter	Present study	Feenstra et al. (1995)	Pettigrew et al. (1989a, b)	Axisa et al. (1985)[a]	Mann and Mayinger (1995)	Hirota et al. (1996)	Nakamura et al. (1999)
Test fluid	R-11	R-11	Air–water	Steam–water	R-12	Steam–water	R-123
P/D	1.485	1.44	1.47	1.44	1.5	1.46	1.46
D (mm)	7.11	6.35	13.0	19.05	22.0	22.2	22.0
f_a (Hz)	35.5	38.1	≈33	≈74	22.5	22.1	20.75
f_L (Hz)	25.5–27.5	≈32.8	≈26.9	≈60	≈17.5	17.9	—
m_t (kg/m)	0.147	0.179	≈0.37	≈0.52	1.60	≈0.87	—
ζ_a	0.03%[b]	0.11%[b]	< 0.2%	≈0.5%	0.11%	≈0.4%	0.1%
ζ_L	0.68%[b]	—	—	—	—	—	—

[a] Tube end conditions are fixed-pinned (all other studies used fixed-free end conditions).
[b] Measurement was made with other tubes held fixed.

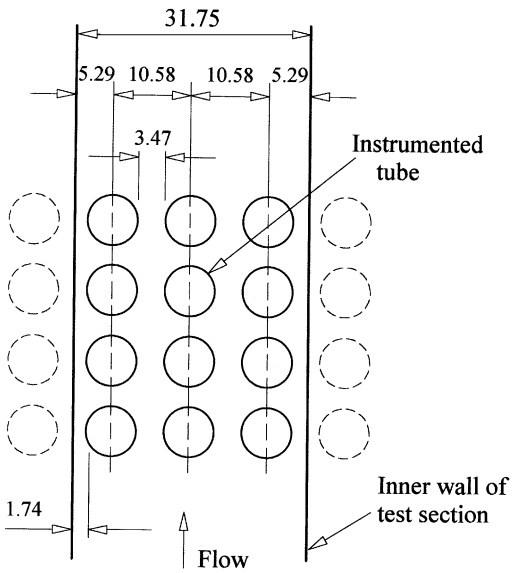

Fig. 1. End view of tube bundle layout (dimensions in mm).

where ρ_G and ρ_L are the gas and liquid densities, respectively, x is the flow quality and S is the slip ratio (or velocity ratio) of the gas and liquid phases such that $S = U_G/U_L$ (see Whalley, 1987). Measurement of slip ratio has traditionally been neglected by many researchers in favour of assuming the HEM, in which the two phases are assumed to be well mixed and flowing with equal velocity. Thus the HEM void fraction, α_H, is determined using Eq. (1) and assuming $S = 1$. A general expression for the time-averaged two-phase fluid density, ρ, is determined by

$$\rho = \alpha\rho_G + (1 - \alpha)\rho_L. \tag{2}$$

Note that we since the flow is adiabatic in the test-section, it is assumed that the density is also spatially averaged in the tube bundle. The HEM fluid density, ρ_H, is determined using Eq. (2) by substituting α_H in place of α. The HEM pitch flow velocity, V_p, is determined by

$$V_p = G_p/\rho_H. \tag{3}$$

The pitch mass flux, G_p, is determined from flow measurements obtained from an orifice plate reading by

$$G_p = (\dot{m}/A_u) * P/(P - D), \tag{4}$$

where $\dot{m}$ is the measured mass flow rate, A_u is the flow area immediately upstream of the tube array, P is the tube pitch, D is the tube diameter.

In two-phase flow, some uncertainty remains on how best to define the average fluid density and flow velocity of the two-phase mixture. The traditional approach has been to use the HEM, which treats the two-phases as well mixed and moving with equal velocity. In a vertical flow however, the gas phase flows faster than the liquid due to buoyancy or gravity effects, and therefore the actual void fraction is lower and the average fluid density is higher than predicted by the HEM. Recently, researchers have been experimenting with newer fluid models that account for the slip ratio, S, between the two phases. To determine slip ratio, one either needs direct measurement of the void fraction of the flow, or an adequate two-fluid model to predict it. In this regard, a new analysis procedure is employed to determine average two-phase fluid density of the present data along with the traditional HEM method. This is afforded by a gamma densitometer, used in the experiments of this study, that permitted an independent measurement of void fraction of the flow in the test-section just upstream of the tube bundle. Thus, a method to more accurately predict the average density of the two-phase mixture was possible in the present study, termed RAD for radiation attenuation determination. For more information on gamma densitometry, see Chan and Banerjee (1981).

In order to properly compare the present RAD data with data of other researchers who did not measure void fraction directly, an empirical model for predicting the void fraction in vertically upward two-phase flows through horizontal tube bundles was used. This model was first introduced by Feenstra et al. (2000b), where it was developed from their R-11 data and tested against other researchers' measurements of time-averaged void fraction for vertical two-phase air–water and R-113 flows through horizontal tube bundles. Remarkably good agreement was observed over a wide range of mass flux and array geometries. The new void fraction model, which predicts the velocity ratio of the phases, is given by

$$S = 1 + 25.7(\mathrm{Ri} * \mathrm{Cap})^{0.5}(P/D)^{-1}, \tag{5}$$

where the velocity ratio, S, is used in conjunction with Eq. (1) to determine the actual void fraction, α. The Richardson number, Ri, is calculated by

$$\mathrm{Ri} = \Delta\rho^2 g a/G_p^2, \tag{6}$$

where a is the gap between the tubes, $\Delta\rho$ is the density difference between the phases (i.e., $\Delta\rho = \rho_L - \rho_G$) and g is the gravitational acceleration. The Capillary number, Cap, is calculated by

$$\mathrm{Cap} = \mu_L U_G/\sigma, \tag{7}$$

where μ_L is the liquid phase absolute viscosity, σ is the liquid surface tension and U_G is the gas phase velocity determined by

$$U_G = xG_p/\alpha\rho_G. \tag{8}$$

While this definition of the Capillary number is unusual, it created the best fit for the slip ratio model and, of course, the liquid and gas phase velocities are related by the slip ratio. This void fraction model is utilized in this paper to obtain more accurate estimates of the time-averaged fluid density of other researchers' data sets for subsequent stability analysis.

In addition to the traditional HEM approach, two new methods of time-averaged flow velocity calculation are considered in this paper. The first new method is designated as an "equivalent" two-phase flow velocity, V_{EQ}, which is

calculated by a summation of the kinetic energy of the two-phases and weighted by the void fraction, α, as given below:

$$V_{EQ} = \sqrt{(\alpha\rho_G U_G^2 + (1-\alpha)\rho_L U_L^2)/\rho}. \tag{9}$$

This is perhaps a more realistic estimate of the effective velocity of the two-phases than the HEM pitch velocity given by Eq. (3). The average density, ρ, and phase velocities, U_L, U_G, are determined either from the RAD analysis (i.e., from gamma densitometer measurements) or from the slip ratio model.

The second new method of flow velocity determination examined in this study is called an "interfacial" flow velocity, V_i, that was first introduced by Nakamura et al. (2000), is given by

$$V_i = 0.73(U_{GS} + U_{LS}) + \sqrt{gD_e(\rho_L - \rho_G)/\rho_L}, \tag{10}$$

where an effective tube diameter is defined as, $D_e = 2(P - D)$. The superficial liquid and gas phase velocities, U_{LS} and U_{GS}, are given by

$$U_{LS} = (1-x)G_p/\rho_L, \quad U_{GS} = xG_p/\rho_G. \tag{11}$$

The specific form of Eq. (10) was adapted from Nicklin et al. (1962), and given final form by correlating it with interfacial velocity measurements obtained from vertical two-phase flows of R-123 and steam–water in horizontal tube bundles as described in Nakamura et al. (2000). Their measurements were obtained using a specially designed bi-optical probe, which could detect the passage of a gas–liquid interface across the probe tip by a change in refractive index of the fluid and hence a change in light intensity reflected back from the probe tips. The velocity was determined by correlating the two signals from the probe tips to determine the average time difference between the passage of an interface from the lower probe tip to the upper one. It should be noted that this correlation was developed from experiments with vertically upward R-123 and steam water flows in a normal square tube array at high void fraction flows of between $\alpha_H = 80$–95%, typical of that in the U-bend region of a nuclear steam generator. Nakamura et al. (2000) assumed that the flow regime would be slug flow and froth flow at these high void fractions.

2.4. Procedure for single-phase flow experiments

Initially, experiments were conducted in single-phase liquid flow, because it was important to establish a benchmark response of the tube bundle in a realm, which is fairly well mapped out by previous research. In this case, it was desired to obtain the vibratory amplitude response of the tube bundle as a function of pitch-flow velocity. This experiment consisted of a many trials where, in each trial, the amplitude response of the monitored tube was measured for a constant pitch-flow velocity. The flow rate in each trial was set and permitted to run for a few minutes to ensure steady flow conditions. The output of the displacement transducer was input to a spectrum analyser, from which vibration amplitude and frequency were determined. The procedure was repeated for increasing flow velocities until tube clashing occurred or was imminent. The single-phase flow experiments were operated at room temperature with no heating of the flow.

2.5. Procedure for two-phase flow experiments

Experience has shown that the tube response in two-phase flow is a function primarily of two variables: mass flux and flow quality (or void fraction). Proper determination of the tube amplitude response requires that one parameter be held constant while the other one is varied. In this study, the flow quality was increased in each trial, starting from zero, while the mass flux was maintained constant. By this method, the flow rate into the test-section was set and held constant while the flow quality was varied from one trial to the next simply by increasing the heater power. Data acquisition was commenced when steady state conditions were achieved, determined by monitoring fluid temperatures at various points around the loop. The r.m.s. tip amplitude of the monitored tube and the frequency spectrum were determined from 100 sample averages, over a frequency range of 0–100 Hz on the dynamic analyser.

The experimental procedure adopted for this study, in which mass flux was held constant while void fraction was varied, was favoured over the reverse approach adopted by other researchers mainly because it required fewer variables to adjust when moving from one trial to the next. Since the flow rate was held constant throughout the experiment, much of the uncertainty in this parameter was eliminated. Visual observations verified that uniform flow conditions with regard to bubble size, void distribution and flow velocity existed across the test-section at FEI for all test cases. Additionally, tube response spectra showed that there was no measurable tube excitation due to the gear pump.

3. Fluidelastic instability in single-phase liquid flow

3.1. Tube bundle response in single-phase liquid cross-flow

The amplitude response of the tube bundle is shown in Fig. 2 for the fully flexible bundle and the single flexible tube bundle. For the fully flexible case shown in Fig. 2(a), symmetric vortex shedding is believed to be the cause of the large drag response that initiated at $V_P = 0.22$ m/s and persisted nearly up to the fluidelastic stability threshold, which occurred at $V_P = 0.52$ m/s. Visual observation of these vortex-induced streamwise tube motions were made with the aid of a strobe light. It was observed that each tube vibrated in phase with its transverse neighbours. By observing each of the four transverse tube rows, it was observed that the lower three transverse tube rows vibrated about 90° out of phase with the neighbouring rows, while the top row vibrated about 180° out of phase with respect to the tube row below. These observations appeared to hold true for the full range of flow velocity in which vortex-induced tube motions were observed.

In the sub-critical region, as shown in Fig. 2(a), the vibration frequency increased gradually from 25.5 Hz up to about 27.5 Hz at the stability threshold. The lift and drag direction frequencies were generally the same for each trial. Beyond the critical flow velocity, the vibration frequency suddenly jumped up to 33 Hz. This behaviour was similar to that observed with the parallel triangular tube bundle of Feenstra et al. (1995), where a sudden jump in frequency from 30.5 to 37.0 Hz was observed in single-phase liquid flow. It is believed that this increase in frequency is due to a reduction in fluid added mass caused by the liquid flashing into vapour on the tube surfaces during vibration.

Experiments were also conducted with all tubes held fixed except for the monitored tube (see Fig. 1). The results for this single flexible tube in a rigid array are shown in Fig. 2(b). The stability threshold is seen to occur at $V_P = 0.66$ m/s which is about 25% higher than for the fully flexible array. The onset of symmetric vortex shedding occurs at

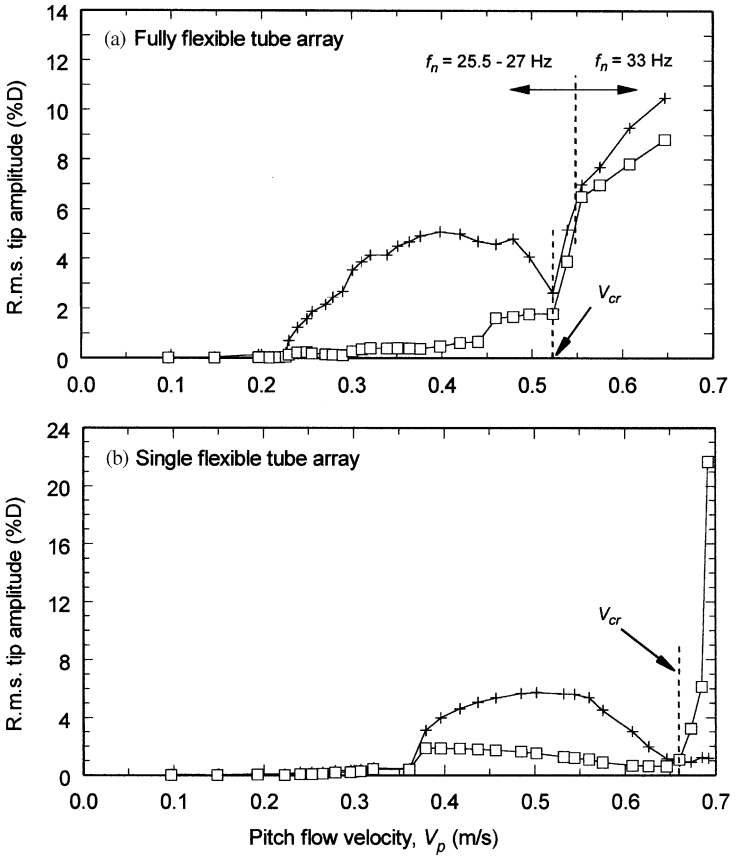

Fig. 2. Amplitude response of the tube array subjected to single-phase liquid R-11 cross-flow. (a) Fully flexible tube bundle, $V_{p,c} = 0.52$ m/s. (b) Single flexible tube with other tubes held fixed, $V_{p,c} = 0.66$ m/s. +, drag direction; □, lift direction.

$V_P = 0.36$ m/s, which is about 70% higher than for the fully flexible array. Interestingly, the peak amplitude in the drag direction in the vortex shedding region was slightly higher than in the fully flexible case (i.e., 6%D. vs. 5%D) The vibration frequency remained fairly constant (in the sub-critical flow range) at roughly 29 Hz, increasing slightly to 30 Hz. Just before the fluidelastic stability threshold was reached, the transverse frequency shifted downward to 28 Hz.

The fact that the stability threshold is slightly delayed for the single flexible tube case indicates that both the displacement mechanism and velocity mechanism are at work to initiate FEI in this tube array. If the stability threshold had been greatly delayed or absent in the case of the single flexible tube bundle, this would indicate that FEI was controlled by a displacement mechanism, in which the dominant fluid forces are proportional to the tube displacement relative to its nearest neighbours. Under this mechanism, the fluid forces act in phase with tube displacement with respect to its nearest neighbours. Chen (1983) concluded that the velocity mechanism (negative damping) is the dominant influence in heavy fluids, such as water and liquid R-11, while fluid stiffness related forces related to the displacement mechanism are dominant in "light" fluids such as air. Such a conclusion would suggest that the threshold flow velocity in a liquid cross-flow should be nearly the same for the single flexible tube case and the fully flexible case. However, the observed delay in the onset of FEI for this tube array is also dependent upon tube pattern, since Feenstra et al. (1995) found that the FEI threshold was the same for the fully flexible and single flexible tube cases of a parallel triangular array in liquid R-11 cross-flow.

3.2. Comparison of results in single-phase flow with other data

The amplitude response of the fully flexible bundle of the present array was compared in Fig. 3 with previous data of Weaver and Abd-Rabbo (1985), who tested a normal square bundle of 25.4 mm diameter acrylic tubes, and data of Weaver and Yeung (1983) who tested a normal square bundle of 12.7 mm diameter aluminium tubes. These other studies were conducted in water cross-flow and the pitch over diameter ratios of those tube bundles were both $P/D = 1.5$. In Fig. 3, the comparison is made on the basis of the reduced pitch flow velocity, V_P/fD, where the vibration frequency at the threshold flow velocity was used as a normalizing parameter as indicated in each graph. The similarity in tube response between the present study and that of Weaver and Abd-Rabbo is remarkable. In both studies, a significant response in the drag direction was observed below the critical velocity at a reduced velocity of about 1.2. Through flow visualization, those authors found that symmetric vortex shedding was the root cause, affecting the second and third tube rows the most. In the post-critical region, above a reduced velocity of about 2.75, both studies revealed that the lift and drag amplitudes are nearly equal, indicating that the tube exhibited a whirling orbit. Weaver and Yeung's work also shows remarkable similarities with the present tube response, though those authors made no distinction between lift and drag response and simply presented the overall amplitude. This comparison of the response of tubes with much different densities and diameters in single-phase flow demonstrates the validity of the results obtained using the present apparatus. In particular, questions regarding the small scale of the present set-up are resolved, at least for characterising the single-phase flow response of the tube bundle. The remarkably long lock-in region is common to all three sets of experiments and is associated with strong fluid–structure coupling as well as shifting relative modes with increasing flow velocity.

For comparison purposes, the fluidelastic threshold flow conditions in single-phase flow for the fully flexible tube bundle case are plotted in Fig. 4 on two separate stability diagrams drawn from the review papers of Weaver and Fitzpatrick (1988) and Chen (1984). These diagrams are presented in the form of reduced velocity, V_P/fD, versus mass damping parameter, $m\delta/\rho D^2$. In order to make the comparison consistent with the other plotted data, the logarithmic decrement of damping of the tube in quiescent air, δ_a, is utilized in the upper graph, while the in-fluid damping, δ_L, is utilized in the lower graph. In this study, tube damping in air was determined by analysis of the amplitude decay trace of the monitored tube after plucking, with the other tubes held fixed. The parameters used to determine reduced velocity and the mass-damping parameter for the monitored tube at the stability threshold in single-phase flow are given in Table 2. The critical reduced velocity is 2.68 and the mass-damping parameter is 0.0062 and, as seen in Fig. 4(a), it shows good agreement with previous empirical results obtained from experiments in single-phase flow of air and/or water. The mass-damping parameter of the present study is rather low when using this methodology because the bundle has very low structural damping, due to the soldered joint between the tubes and the brass mounting block. For the single flexible tube in the rigid array, the critical reduced velocity is 3.32 and the mass-damping parameter is 0.0060. These data are also plotted in Fig. 4(a), where it lies above and slightly to the left of the data-point of the fully flexible bundle. Comparison of the data using the stability diagram provided by Chen (1984) is shown in Fig. 4(b). The critical reduced velocity for the fully flexible case remains 2.68, and the mass-damping parameter is 0.139. The data agrees well with previous data.

The purpose of comparing the single-phase fluidelastic threshold data to that of others was to provide benchmark response characteristics of the present tube bundle. It is important that the amplitude and frequency response in

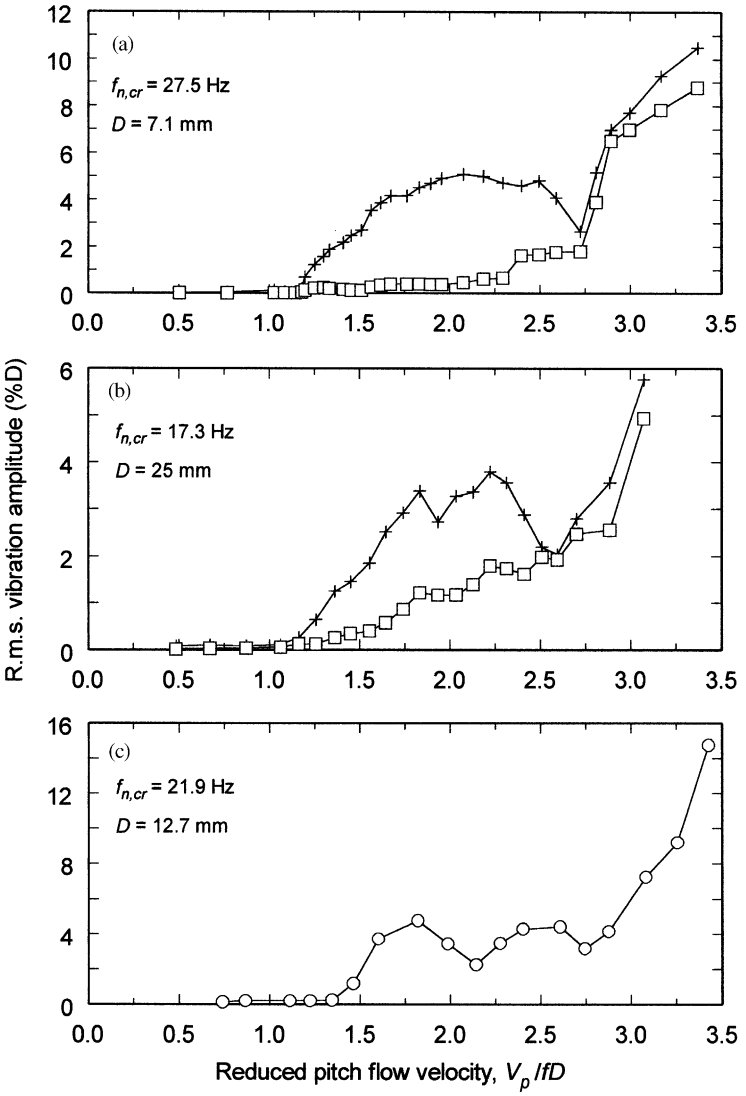

Fig. 3. Comparison of amplitude response data for single-phase liquid cross-flow. (a) Present data, (b) Weaver and Abd-Rabbo (1985), (c) Weaver and Yeung (1983). +, drag direction; □, lift direction; ○, overall amplitude.

single-phase cross-flow should agree with previously published data since knowledge in this field is relatively sound. The results of these tests provide a basis for interpreting the subsequent vibration tests in two-phase cross-flow.

4. Fluidelastic instability in two-phase flow

4.1. Tube bundle response in two-phase cross-flow

The following sections describe the experimental results for FEI in two-phase R-11 flow, where the primary purpose was to determine the threshold velocity for the onset of FEI in a two-phase flow of varying void fractions and mass fluxes. A comparison is made between two methods of data analysis, the traditionally used HEM vs. the slip ratio analysis, which was afforded by the gamma densitometer measurements and the void fraction model introduced by Feenstra et al. (2000b). The amplitude response and fluidelastic threshold data of the fully flexible tube bundle are presented along with damping measurements obtained from the single flexible tube array.

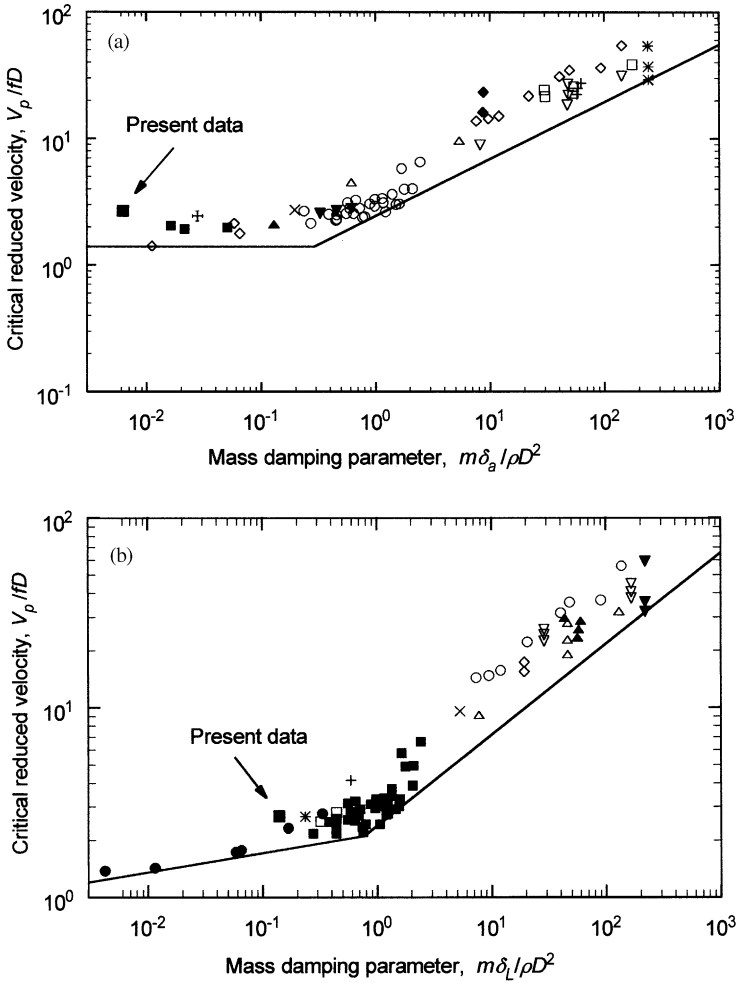

Fig. 4. Critical flow velocities for FEI of normal square tube arrays in cross-flow. (a) Stability diagram drawn from Weaver and Fitzpatrick (1988) utilizing in-air damping. (b) Stability diagram drawn from Chen (1984) utilizing in-liquid damping. ■, Present data in liquid R-11 cross-flow.

Table 2
Summary of fluidelastic instability data for single-phase R-11 cross-flow

Parameter	Present study Normal square tube bundle, $P/D = 1.485$		Feenstra et al. (1995) Parallel triangular tube bundle, $P/D = 1.44$	
	Fully flexible tube bundle	Single flexible tube bundle	Fully flexible tube bundle	Single flexible Tube bundle
$V_{p,c}$ (m/s)	0.52 m/s	0.66 m/s	0.32 m/s	0.34 m/s
f (Hz)	27.5 Hz	28.0 Hz	29.4 Hz	31.8 Hz
$V_{p,c}/fD$	2.68	3.32	1.71	1.68
m (kg/m)	0.245 kg/m	0.236 kg/m	0.301 kg/m	0.257 kg/m
ρ_L	1478 kg/m^3	1473 kg/m^3	1477 kg/m^3	1477 kg/m^3
δ_a[a]	0.0019	0.0019	0.0069	0.0069
$m\delta_a/\rho D^2$	0.0062	0.0060	0.035	0.030
δ_L[a]	0.0425	0.0425	—	—
$m\delta_L/\rho D^2$	0.139	0.135	—	—

[a] In-air and in-liquid damping values obtained from instrumented tube with other tubes held fixed.

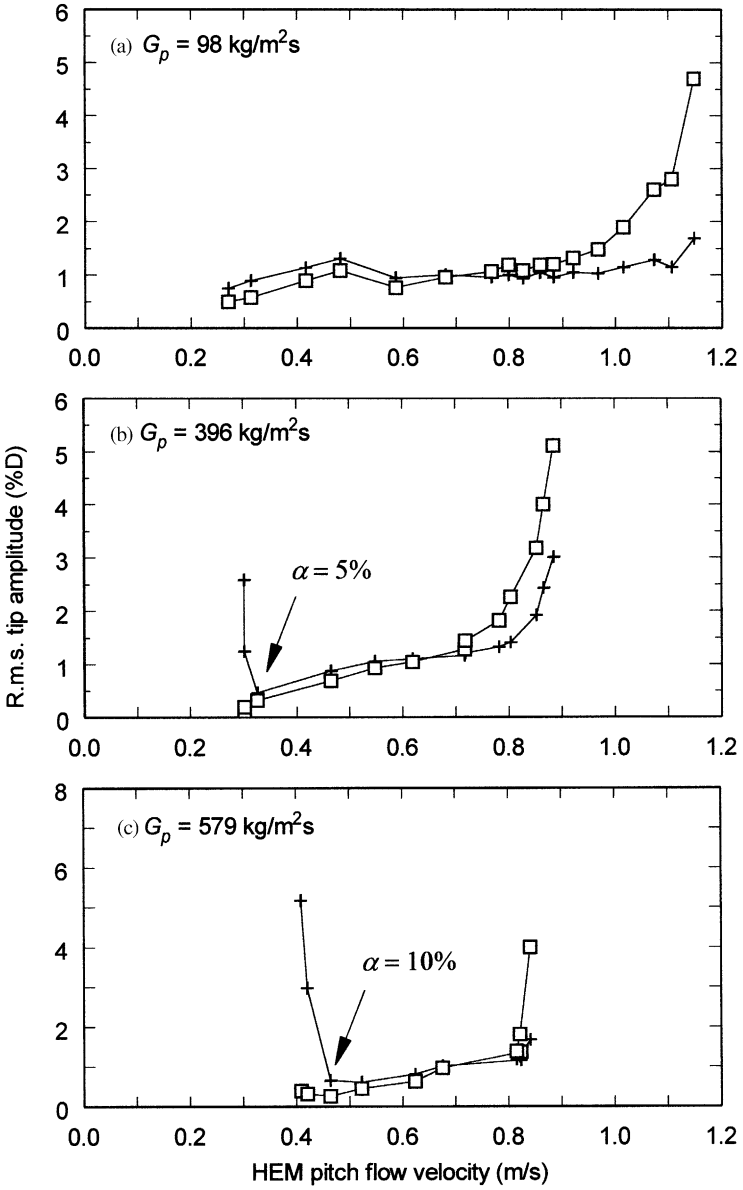

Fig. 5. Amplitude response of the fully flexible tube array subjected to two-phase R-11 cross-flows of pitch mass fluxes of (a) $G_p = 98\,\mathrm{kg/m^2s}$, (b) $396\,\mathrm{kg/m^2s}$, (c) $579\,\mathrm{kg/m^2s}$. +, drag direction; □, lift direction.

Fig. 5 presents a sample of amplitude response curves of the monitored tube for the flexible array, which illustrates the phenomenon of FEI in two-phase flow. The graphs show the r.m.s. tip amplitude of the tube versus HEM pitch flow velocity which is calculated by Eq. (3). Each graph corresponds to a different pitch mass flux, which is held constant while the void fraction is varied from zero. Below the critical two-phase flow velocity, the tube responds to turbulence, gradually increasing in amplitude as the effective flow velocity increases. Beyond this however, the vibration amplitude increases at a much greater slope, particularly in the lift direction. This change in response behaviour and amplitude vs. velocity slope is defined as the fluidelastic threshold. The threshold is particularly well defined at high-mass fluxes such as seen in Fig. 5(c) but is less clear at low-mass fluxes such as shown in Fig. 5(a). In such cases, the critical threshold was determined as the point when the slope of the curve starts to deviate significantly away from that of the turbulence-buffeting region.

Of particular interest are the high values of streamwise response at the lowest velocities in Figs. 5(b) and (c). These are associated with symmetric vortex shedding in liquid flow as discussed in relation to Fig. 3. Recall that increasing the

HEM pitch flow velocity in Fig. 5 is caused by heating the fluid and thereby generating vapour bubbles in the flow. Thus, the dramatic reduction of vibration amplitude in Figs. 5(b) and (c), at about 0.31 and 0.43 m/s, respectively, are due to vapour in the flow, where the void fraction is indicated by the percentage values in those figures. These observations are very important because they demonstrate that a small amount of vapour in the flow is sufficient to disrupt vortex excitation of tube arrays and help justify the neglect of vortex shedding response for tube arrays in two-phase flows.

4.2. Comparison of FEI results in two-phase flow with other data

The results of the present study for FEI are plotted in Fig. 6 along with data sets other researchers who tested normal square arrays using a variety of modelling fluids: Pettigrew et al. (1989b) in air–water; Mann and Mayinger (1995) in

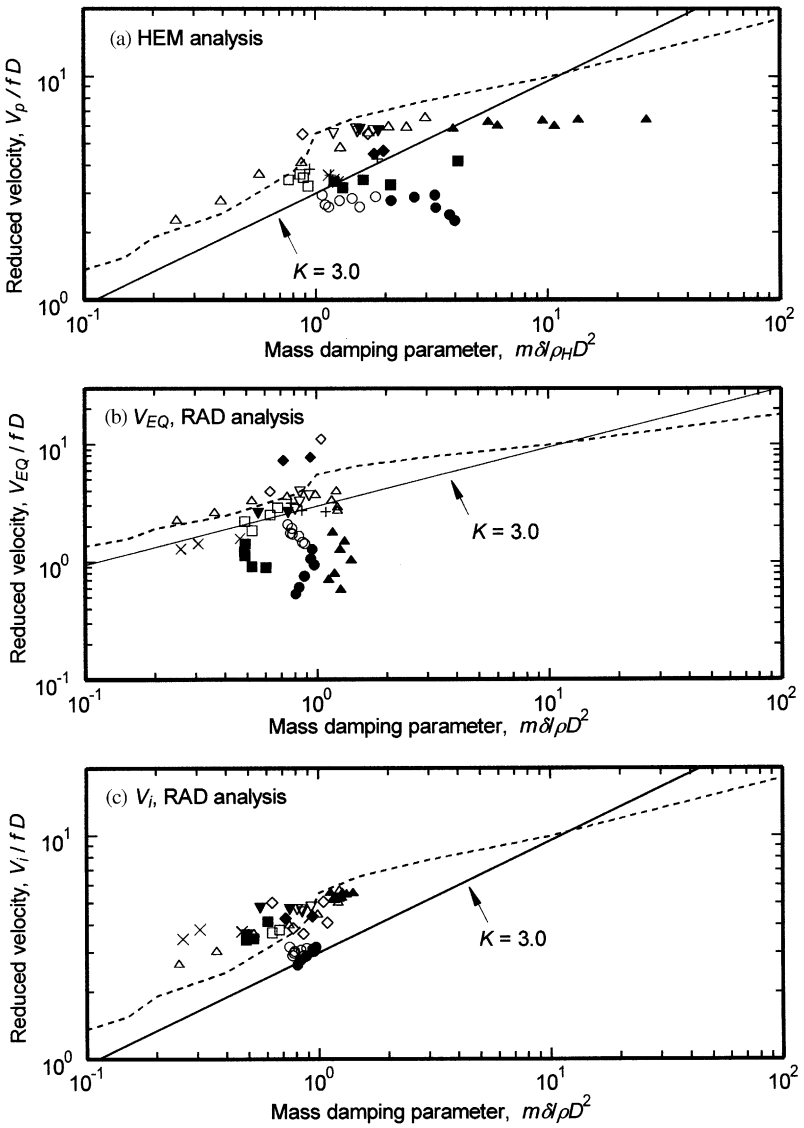

Fig. 6. Critical flow velocities for FEI of normal square tube arrays in two-phase cross-flows. Data analysed by (a) HEM, (b) V_{EQ} and RAD, (c) V_i and RAD. □ ■, Present study in R-11; ○ ●, Feenstra et al. (1995) in R-11 (parallel triangular array); △▲, Pettigrew et al. (1989b) in air–water; ▽▼, Axisa et al. (1985) in steam–water; +, Mann and Mayinger (1995) in R-12; ◇ ◆, Hirota et al. (1996) in steam–water; ×, Nakamura et al. (1999) in R-123;———, Connors' theory; - - - - - - -, prediction of Li & Weaver (1997). ○△▽□+, Bubbly flow; ●▲▼■◆, intermittent flow; ▼, dispersed flow.

R12; Axisa et al. (1985) in steam–water, Hirota et al. (1996) in steam–water and Nakamura et al. (1999) in R-123. The present results are also compared with the fluidelastic data for the parallel triangular array of Feenstra et al. (1995) in this figure. The theoretical prediction of the well-known Connors model is also plotted as is the theoretical prediction of Li and Weaver (1997) for parallel triangular arrays for single-phase flow. The data are presented on graphs, which feature critical reduced velocity versus mass-damping parameter. These are currently believed to be the two most important dimensionless parameters for scaling the phenomenon of FEI, while array geometry and pitch ratio are also important. In the upper graph, Fig. 6(a), the dimensionless parameters are calculated using the traditional HEM. In the lower graphs, Figs. 6(b) and (c), the RAD measurements and/or the void fraction model of Feenstra et al. (2000b) are used to calculate the average fluid density and new correlations for two-phase flow velocity, V_{EQ} and V_i, are used. These fluidelastic threshold data are also summarized in Table 3.

The in-flow damping value, ζ, measured at roughly half the mass flux for FEI, was used to plot the data of the present study. This was done to be consistent with the analysis methods of Pettigrew et al. (1989b). The lower bound Connors' constant, $K = 3.0$ was determined by Pettigrew et al. (1989b) for P/D ratios of between 1.4 and 1.5 in continuous flow regimes (bubbly). The constant, K, follows from the often-quoted Connors' relationship

$$V_{p,c}/fD = K\sqrt{2\pi\zeta m/\rho D^2}. \tag{12}$$

This theory predicts that the critical reduced velocity should rise proportionally with mass-damping parameter to the one-half power. The data-points in Fig. 6(a) are distinguished between the different flow regimes predicted by the map of Ulbrich and Mewes (1994). The open symbols correspond to bubbly flow and the solid symbols represent intermittent flow (or dispersed flow for the data-points of Axisa et al.).

The present data in Fig. 6(a) shows a slightly lower stability threshold than the other data of the normal square array type. It is clear that the parallel triangular bundle shows the lowest stability, where a lower bound Connor's constant of $K = 2.0$ is appropriate if one considers only the data corresponding the bubbly flow regime. When one considers all the data of Feenstra et al. (1995), then a lower bound constant of $K = 1.1$ seems to apply. When plotted in this way, however, it is clear that the data trend for intermittent flow does not follow that suggested by Connors' equation.

Figs. 6(b) and (c) shows the same data sets as in the upper graph but with two differences in data reduction. The first is that the average two-phase fluid density for the present data and that of Feenstra et al. (1995) were determined from the void fraction measurements obtained with the gamma densitometer. However, since the studies of Pettigrew et al. (1989b) and Axisa et al. (1985) had no means of making a direct void fraction measurement, the average density for their data is estimated using the void fraction model of Feenstra et al. (2000b). The second difference is how the average two-phase flow velocity is determined for the analysis. In Fig. 6(b), the equivalent flow velocity, V_{EQ}, is used to determine the critical reduced flow velocity, while in Fig. 6(c), the interfacial flow velocity, V_i, is used. Note that the mass per unit length, m, and the vibration frequency, f, remained unchanged in the modified analysis. As was done in Fig. 6(a), each data set in Figs. 6(b) and (c) are differentiated by the predicted flow regimes.

By comparing Fig. 6(b) with 6(a) it is clear that the new void fraction ratio model has compressed each data set into a smaller range of mass-damping parameter. Because the RAD void fraction measurement and the void fraction model always predict a lower void fraction than the HEM, this affects the determination of average fluid density, so that ρ is always higher than ρ_H. More importantly however, the overall range of average density for each data set is shrunk when the new void fraction modelling technique is applied. In Fig. 6(b), the air–water data shows a remarkable change in behaviour between the predicted bubbly and intermittent flow regimes. In bubbly flow, the critical reduced velocity results follow a trend with mass-damping parameter, which roughly agrees with Connors' formula. However, the data-points corresponding to the intermittent flow regime show a significant reduction in critical reduced velocity over a small range of mass-damping parameter. Roughly the same observation was observed for data of the present study data. The steam–water data of Axisa et al. (1985) is rather tightly clustered in both graphs and it is difficult to observe any clear trends in stability behaviour, either with mass-damping parameter or flow regime. The R-11 data of the Feenstra et al. (1995) shows little variation in mass-damping parameter, yet it covers a significant range of reduced velocity.

The application of the interfacial velocity correlation, V_i, is explored in Fig. 6(c). The average fluid density is determined by either the RAD void fraction measurements or from the void fraction model, while the interfacial velocity, V_i, is used to determine the two-phase flow velocity. It is evident that the data appears to show good collapse that coincidentally agrees with Connor's criteria with a constant of $K = 3.0$. In the vertical direction, the data has changed by a small amount when compared to the HEM analysis because there is close agreement between V_P and V_i which can be verified by comparing V_P/fD versus V_i/fD in Table 3. The interfacial velocity is higher than V_P for a flow quality less than 5%. Above a flow quality of about 5%, V_i is slightly lower than V_P. This trend is somewhat intuitive when considering that the correlation for V_i was derived from measurements of a bi-optical probe. For example, at low

Table 3
Summary of fluidelastic instability data for various arrays in two-phase flow

Test	G_p	x	α_H	α	f	ζ	m	HEM model		Slip ratio model		
No.	(kg/m^2)		(%)	(%)	(Hz)	(%)	(kg/m)	$m\delta/\rho_H D^2$	V_p/fD	$m\delta/\rho_H D^2$	V_i/fD	V_{EQ}/fD
Present study, $R-11$, normal square array, $P/D=1.485$, $D=0.00711$ m, $f_a=35.5$ Hz, $\zeta_a=0.03\%$												
A	98	0.1150	94.0	54.0	34.0	2.0	0.160	4.13	4.20	0.603	4.14	0.90
B	150	0.0480	87.3	46.6	33.8	2.0	0.163	2.11	3.27	0.525	3.45	0.92
C	208	0.0379	83.0	42.5	33.8	2.0	0.163	1.61	3.44	0.490	3.59	1.14
D	249	0.0248	77.6	38.4	33.5	2.0	0.165	1.31	3.18	0.486	3.41	1.23
E	288	0.0251	75.5	38.6	33.5	2.1	0.165	1.21	3.38	0.491	3.55	1.43
F	396	0.0145	63.8	35.3	33.0	2.1	0.170	0.93	3.23	0.526	3.46	1.85
G	490	0.0115	57.8	33.3	33.0	2.3	0.170	0.77	3.44	0.489	3.61	2.21
H	579	0.0088	50.2	29.4	32.5	2.9	0.175	0.89	3.52	0.630	3.68	2.50
I	691	0.0062	42.2	26.6	32.3	3.2	0.178	0.86	3.65	0.678	3.79	2.89
Feenstra et al. (1995), R-11, parallel triangular array, $P/D=1.44$, $D=0.00635$ m, $f_a=38.1$ Hz, $\zeta_a=0.11\%$												
F01	478	0.0080	52.0	31.3	36.8	2.50	0.190	1.07	2.95	0.749	2.63	2.08
F02	425	0.0086	53.5	34.3	37.0	2.52	0.188	1.10	2.67	0.782	2.77	1.92
F03	396	0.0088	55.2	33.3	37.0	2.53	0.188	1.14	2.60	0.771	2.89	1.76
F04	389	0.0101	58.5	32.8	36.8	2.57	0.190	1.27	2.78	0.786	3.17	1.73
F05	356	0.0118	63.2	36.2	37.0	2.63	0.188	1.44	2.84	0.837	3.10	1.66
F06	308	0.0132	65.5	37.7	37.0	2.66	0.188	1.55	2.60	0.867	3.03	1.47
F07	296	0.0162	70.1	38.0	37.0	2.71	0.188	1.82	2.89	0.887	3.12	1.43
F08	250	0.0188	73.9	41.6	37.0	2.76	0.188	2.12	2.78	0.957	2.91	1.29
F09	205	0.0256	79.1	42.4	37.0	2.77	0.188	2.63	2.88	0.975	3.07	1.09
F10	176	0.0311	83.1	41.4	37.0	2.82	0.188	3.28	2.95	0.973	3.04	0.95
F11	130	0.0392	85.7	44.7	37.0	2.41	0.188	3.30	2.59	0.882	2.90	0.76
F12	98	0.0458	88.6	46.2	37.0	2.24	0.188	3.79	2.41	0.838	2.97	0.61
F13	86	0.0493	89.3	45.2	37.0	2.22	0.188	3.99	2.26	0.810	3.17	0.54
Pettigrew et al. (1989b), air–water, 22°C, normal square array, $P/D=1.47$, $D=0.013$ m, $f_a=33$ Hz, $\zeta_a=0.2\%$												
O-2	753	6.28E−5	5	3.0	26.9	1.3	0.50	0.25	2.27	0.250	2.65	2.23
O-3	826	2.11E−4	15	9.3	27.0	1.8	0.49	0.39	2.76	0.363	3.01	2.60
O-4	984	3.98E−4	25	16.6	27.7	2.5	0.47	0.57	3.64	0.525	3.63	3.28
O-5	1013	5.61E−4	32	21.8	27.9	3.4	0.46	0.87	4.11	0.745	3.96	3.58
O-6	898	1.19E−3	50	35.2	28.9	4.0	0.43	1.28	4.78	0.989	4.42	3.70
O-7	840	1.79E−3	60	43.4	28.9	4.3	0.43	1.70	5.58	1.216	5.01	3.96
O-8	581	3.57E−3	75	55.0	30.1	3.5	0.40	2.07	5.93	1.160	5.22	3.31
O-9	466	4.75E−3	80	58.7	30.2	3.4	0.40	2.47	5.91	1.227	5.21	2.89
O-10	389	6.72E−3	85	63.4	30.4	3.1	0.39	2.98	6.53	1.230	5.65	2.71
O-11	234	0.0106	90	66.2	30.6	2.8	0.38	3.93	5.83	1.170	5.13	1.77
O-12	176	0.0156	93	69.2	30.6	2.8	0.39	5.56	6.25	1.318	5.43	1.48
O-13	147	0.0184	94	69.7	30.9	2.7	0.38	6.11	6.00	1.258	5.25	1.26
O-14	104	0.0278	96	71.9	30.7	2.8	0.38	9.56	6.34	1.407	5.50	1.02
O-15	75	0.0372	97	72.3	31.0	2.4	0.37	10.77	5.98	1.192	5.23	0.79
O-16	55	0.0553	98	74.3	31.3	2.1	0.37	13.64	6.39	1.122	5.53	0.70
O-17	29	0.1060	99	76.1	31.4	2.2	0.37	26.75	6.38	1.266	5.50	0.58
Axisa et al. (1985), steam–water, 210°C, normal square array, $P/D=1.44$, $D=0.019$ m, $f_a=74$ Hz, $\zeta_a=0.5\%$												
A	244	0.340	97.8	91.5	76.0	0.5	0.526	1.56	5.80	0.560	4.75	2.60
B	321	0.250	96.7	89.5	75.4	0.8	0.529	1.87	5.71	0.751	4.69	2.64
C	420	0.186	95.3	87.6	74.5	1.0	0.532	1.78	5.71	0.807	4.68	2.82
D	638	0.117	92.1	84.0	74.0	1.3	0.540	1.52	5.67	0.843	4.66	3.25
E	828	0.090	89.7	81.8	73.9	1.6	0.546	1.50	5.82	0.927	4.78	3.68
E	1131	0.059	84.7	76.7	73.7	1.8	0.559	1.20	5.56	0.848	4.56	3.95
Mann and Mayinger (1995), R-12, normal square array, $P/D=1.5$, $D=0.022$ m, $f_a=22.5$ Hz, $\zeta_a=0.5\%$												
1	989	0.0754	64.0	35.8	21.7	3.99	1.72	1.85	4.27	1.09	4.07	2.66
2	1205	0.0340	43.0	22.2	20.7	3.44	1.89	1.16	3.62	0.86	3.65	2.74
3	1411	0.0209	32.0	16.0	19.3	2.89	2.18	0.94	3.84	0.78	3.87	3.18

Table 3 (*continued*)

Test	G_p	x	α_H	α	f	ζ	m	HEM model		Slip ratio model		
No.	(kg/m^2)		(%)	(%)	(Hz)	(%)	(kg/m)	$m\delta/\rho_H D^2$	V_p/fD	$m\delta/\rho_H D^2$	V_i/fD	V_{EQ}/fD
Hirota et al. (1996), Steam–water, normal square array, $P/D = 1.46$, $D = 0.0222$ m, $f_a = 22.1$ Hz, $\zeta_a \approx 0.4\%$												
S16a	599	0.0836	70	56.3	19.6	1.42	1.221	0.88	5.51	0.630	5.03	3.99
S16b	423	0.1353	80	65.3	19.5	1.90	1.233	1.69	5.54	1.048	5.05	3.55
S16c	216	0.2603	90	74.6	20.3	1.40	1.138	1.97	4.65	0.939	4.36	2.50
S16d	118	0.4842	96	84.0	20.0	0.71	1.172	1.79	4.49	0.719	4.27	2.35
Nakamura et al. (1999), R-123, normal square array, $P/D = 1.46$, $D = 0.0222$ m, $f_a = 20.75$ Hz, $\zeta_a \approx 0.1\%$												
A1-1	158	0.4078	95.0	61.6	20.0	1.20	0.867	1.25	3.37	0.260	3.44	1.29
A1-2	265	0.2459	90.0	52.8	19.9	1.70	0.875	1.14	3.62	0.308	3.80	1.43
A1-3	429	0.1266	80.0	42.5	19.6	3.00	0.902	1.20	3.44	0.466	3.72	1.58

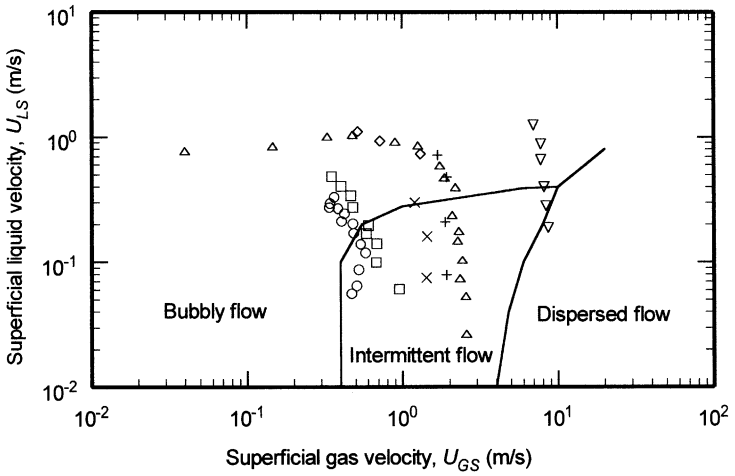

Fig. 7. Flow regime map developed by Ulbrich and Mewes (1994). Fluidelastic threshold data of: □, present study in R-11; ○, Feenstra et al. (1995) in R-11; △, Pettigrew et al. (1989b) in air–water; ▽, Axisa et al. (1985) in steam–water; +, Mann & Mayinger (1995) in R-12; ◇, Hirota et al. (1996) in steam–water, ×, Nakamura et al. (1999) in R-123.

flow quality (or low void fraction) the bi-optical probe would sense the passage of vapour bubbles, which would travel faster than the bulk liquid due to buoyancy. However, at a higher flow quality, the probes would sense the passage of liquid slugs or droplets, which would travel slower than the predominantly vapour phase since the forces carrying the liquid upward against gravity would be due to the drag force of the faster upward flowing vapour.

The overall outcome of the two-phase fluidelastic stability analysis is that a remarkable collapse of the data is obtained in Fig. 6(c), mostly by using the void fraction model of Feenstra et al. (2000b) to determine the average two-phase density and partly by implementing the interfacial velocity model introduced by Nakamura et al. (2000).

4.3. Flow regime

The FEI data presented in the previous section were subdivided between different flow regimes: bubbly, intermittent and dispersed. A vertical flow of two-phase gas and liquid will assume various flow patterns and distribution of phases depending mostly upon the flow quality, the density ratio of the two phases and the total mass flux. The map used to predict the various flow patterns in this work is drawn from Ulbrich and Mewes (1994), and is presented in Fig. 7. The abscissa and ordinate are in terms of the superficial gas and liquid phase velocities respectively, U_{LS} and U_{GS}, defined in Eq. (11). The solid lines in Fig. 7 represent transition boundaries determined by Ulbrich and Mewes, who performed an exhaustive analysis of available flow regime data in vertical two-phase cross-flow through horizontal tube bundles. They

found that the flow patterns observed and those plotted on the traditionally used maps of Taitel et al. (1980) and Grant and Murray (1972), showed only a 46% and 50% rate of agreement, respectively. Consequently, they developed a flow pattern map more appropriate for cross-flow in a tube bundle, with a new set of boundaries, which had an 86% rate of agreement with data from the literature. However, the flow regime boundaries must be considered as approximate, and might be represented better by shaded bands to emphasize the gradual transition that occurs with the flow behaviour when crossing from one flow regime to another. Plotted in Fig. 7 are the flow regime data of the present study together with data from the literature: Pettigrew et al. (1989b, 1995), Axisa et al. (1985), Feenstra et al. (1995), Mann and Mayinger (1995), Hirota et al. (1996), and Nakamura et al. (1999). These data-points correspond to flow conditions at the stability threshold for FEI. Most of these data sets appear to cross over from the bubbly to the intermittent flow regimes. This is of particular interest because the previous analysis (see Fig. 6a) suggested that a different fluidelastic behaviour existed between the data in these two flow regimes.

4.4. Damping measurements

The structural damping of the monitored tube in the bundle, ζ_a, was obtained by plucking the tube in air and capturing the amplitude decay trace at a sampling rate of about 15 times the vibration frequency. Care was taken during plucking to excite only the lowest cantilever mode. This was performed with the bundle mounted in a heavy vise, and with the other tubes held secure so that the energy of the monitored tube would not "leak" away to other tubes. The vibration was monitored by the optical light probe (same as that used in the experiments) for the lift and drag directions separately. The damping was calculated using special FORTRAN software that fits an "envelope" curve to the amplitude decay trace and calculates the equivalent logarithmic decrement damping, δ_a, from which the damping ratio is calculated by $\zeta_a = \delta_a/2\pi$. This program provides damping values and corresponding amplitudes, so that the damping value at an r.m.s. amplitude of 2% of the tube diameter (i.e., 2%D) was retained for analysis. The results in the lift direction for three trials showed good agreement at a damping ratio of $\zeta_a = 0.03\%$, and there was little variation of damping over an r.m.s. amplitude range of 1.5–3.5%D.

Damping measurements were also made in still liquid R-11. The tube bundle was mounted in the test-section, with all tubes fixed except the instrumented tube. This was accomplished by inserting a thin metal plate over the free ends of the tubes with a hole pattern the same as the bundle. The hole for the monitored tube was oversize to allow this tube to vibrate. This configuration is also known as the "single flexible tube bundle". The test-section was moderately impacted to excite the tubes in the lift direction. The amplitude decay trace was captured by the optical light probe for later analysis using the FORTRAN software. In this case, an average damping value for still liquid R-11 of $\zeta_L = 0.68\%$ was obtained. This data can be found in Table 1.

Damping measurements in two-phase flows were obtained in-flow using the single flexible tube bundle. To be consistent with the method of Pettigrew et al. (1989a, 1995), care was taken to obtain damping measurements at critical values of HEM void fraction but at half the critical mass flux for FEI (i.e., "critical" refers to flow conditions at the threshold of FEI). The original logic behind this approach was that, since damping appeared to vary mostly with void fraction and little with mass flux (as observed in the air–water study of Pettigrew et al., 1989a), representative damping values could be obtained from additional experiments with a single flexible tube bundle subjected to conditions at the critical HEM void fraction but at lower mass flux. It was thought that such an approach would avoid fluidelastic forces, which would violate the assumptions that were required for half-power bandwidth analysis: i.e., that the forcing must be random and ergodic.

The damping data for this study are presented in Fig. 8 as a function of HEM void fraction. These data-points were obtained from the monitored tube, averaged over 100 samples of the spectral analyser and a frequency resolution of 0.25 Hz. Damping values were determined from a best fit of a frequency response function to the measured frequency spectra using special FORTRAN software written by AECL. The damping values plotted in Fig. 8 represent an average of the lift and drag directions where, in most cases, the drag direction damping was slightly higher. Each curve on this graph represents a particular experiment in which the mass flux was held constant while the void fraction was increased from one trial to the next. On each of these curves, a circle indicates the desired conditions for obtaining representative damping data for FEI analysis (i.e., conditions at the critical HEM void fraction but at half the critical mass flux). The solid lines indicate that the damping increases with void fraction (for the range that was tested), but the trend of the representative data-points (indicated by the larger circles) suggests the opposite, that damping decreases with void fraction. This apparent contradiction underscores the difficulty in obtaining reliable damping data for tube bundles in two-phase flows. Additionally, while the damping values obtained at one-half the critical mass flux may be useful for practical stability analysis, the use of such data to estimate the two-phase damping at the stability threshold seems difficult to justify scientifically. It should be noted that the damping data shown in Fig. 8 extends only over a limited

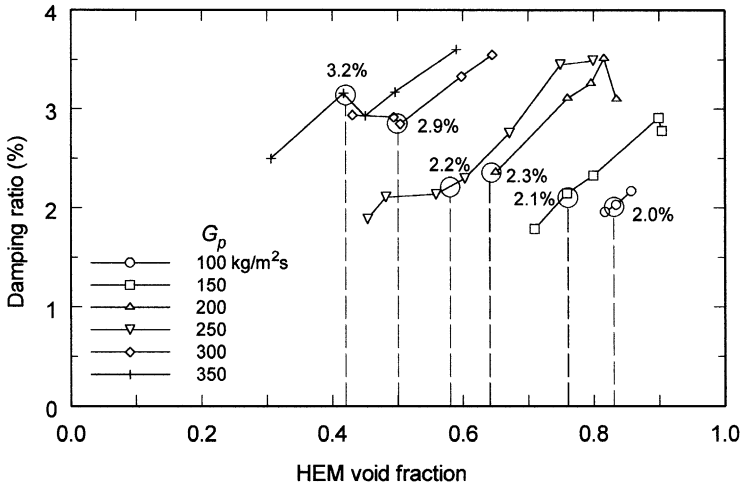

Fig. 8. Summary of damping measurements of the present study for the single flexible tube bundle subjected to two-phase cross-flow. Data curves correspond to a nominal pitch mass flux of: ○, $G_p = 100\,\mathrm{kg/m^2s}$; □, $150\,\mathrm{kg/m^2s}$; △, $200\,\mathrm{kg/m^2s}$; ▽, $250\,\mathrm{kg/m^2s}$; ◇, $300\,\mathrm{kg/m^2s}$; +, $350\,\mathrm{kg/m^2s}$.

range of pitch mass flux between $G_p = 100$ and $350\,\mathrm{kg/m^2\,s}$. Conditions below this range are unattainable because it is not practical to operate the flow-loop at a pitch mass flux below $100\,\mathrm{kg/m^2\,s}$.

5. Conclusions

FIV experiments were conducted to explore the response of a normal square array of tubes subjected to single- and two-phase cross-flows. The tube bundle consisted of 12 cantilevered tubes, with a tube diameter of 7.11 mm and a pitch over diameter ratio of $P/D = 1.485$. Refrigerant 11 was the working fluid, in which the vapour phase was generated by boiling on electric heater elements. A gamma densitometer was used to make void fraction measurements in the test-section just upstream of the tube bundle. Damping measurements of the tube vibration in two-phase flow were made with the all tubes in the bundle fixed except the monitored tube. The primary intent of this work was to determine the threshold flow velocity for the onset of FEI. Of special interest was to compare the present data with that of a parallel triangular tube bundle that was studied previously in the same apparatus. Comparison was also made with other researchers' data using a variety of techniques for determining average fluid density and average pitch flow velocity in two-phase flow. A summary of findings of this study are as follows:

1. The amplitude response of the tube bundle in single-phase liquid flow was very similar to that of other normal square tube arrays in liquid flows such as: Weaver and Abd Rabbo (1985), who tested a bundle of 25 mm diameter acrylic tubes, and Weaver and Yeung (1983), who studied a bundle of 12.7 mm diameter aluminium tubes, both in water flows. The amplitude response of the present array was essentially the same as those other bundles. Moreover, when plotted on the traditional stability diagram, the present data for FEI showed good comparison with other data in single-phase flows. This finding demonstrated the validity of the reduced scale modelling of the present study, at least in the realm of single-phase flow.
2. In liquid flow, the in-line square arrays show a large peak in response amplitudes below the stability threshold associated with symmetric vortex shedding. The introduction of a small amount of void is sufficient to disrupt this excitation mechanism. This helps to explain why vortex-shedding excitation is not observed to be a problem in two-phase flows.
3. Experiments with a single flexible tube in an otherwise rigid tube bundle showed that the onset of FEI was reached at a flow velocity 25% higher than for the fully flexible tube bundle, while the onset of symmetric vortex shedding occurred at a flow velocity that was 50% higher. This indicates that FEI in single-phase flow for this bundle is controlled by both a displacement mechanism (negative stiffness) and by a velocity mechanism (negative damping). This differs from the response of the parallel triangular tube bundle (tested in the same rig), where the critical velocity was the same for both the single flexible and fully flexible tube cases.

4. The FEI threshold of the tube bundle in two-phase flows was determined in a series of nine tests. In each test, the tube bundle was subjected to a flow of constant mass flux while flow quality was increased from one steady state trial to the next. The amplitude response showed no obvious vortex shedding, but FEI was observed in all of the experiments with the fully flexible tube bundle. Instability was not observed for the single flexible tube bundle in two-phase flow, indicating that the controlling mechanism of FEI for this in-line square array in two-phase flow is dominated by a displacement mechanism (negative stiffness), i.e., coupling with neighbouring tubes.
5. The two-phase FEI data was analysed using the interfacial velocity correlation introduced in Nakamura et al. (2000). The velocity determined by this model showed close agreement with that of the homogeneous equilibrium model. When other fluidelastic data were compared with this model and using the density determined by the RAD void fraction or the void fraction model introduced by Feenstra et al. (2000b), the data showed remarkable collapse in terms of reduced flow velocity and there was good agreement with Connors' model with $K = 3.0$. Moreover, this analysis approach removes the apparent change in stability behaviour seen in the conventional HEM analysis when the flow regime changes from bubbly to intermittent.

Acknowledgements

This paper presents the results of a joint research project between Mitsubishi Heavy Industries and McMaster University.

Appendix A. Nomenclature

a	gap between tubes (m) (i.e., $a = P - D$)
A_u	upstream cross-sectional area of test-section (m^2)
Cap	Capillary number
D	tube diameter (m)
D_e	effective tube diameter (m) (i.e., $D_e = 2(P - D)$)
f	frequency of vibration (Hz)
FEI	fluidelastic instability
FIV	flow-induced vibration
G_p	pitch mass flux ($kg/m^2\,s$)
g	gravitational acceleration (m/s^2)
K	Connors' constant
m	tube mass per unit length including added fluid mass (kg/m)
m_t	tube mass per unit length (kg/m)
Ri	Richardson number
S	slip ratio
U_G	time-averaged gas phase velocity (m/s)
U_L	time-averaged liquid phase velocity (m/s)
U_{GS}	Superficial gas phase velocity (m/s)
U_{LS}	Superficial liquid phase velocity (m/s)
V_P	pitch flow velocity (determined with the HEM) (m/s)
V_i	interfacial flow velocity (m/s)
x	flow quality
α	void fraction
$\Delta\rho$	density difference between phases (kg/m^3)
Δ	Logarithmic decrement damping
ζ	damping ratio
μ	absolute viscosity (Pa s)
ρ	fluid density (kg/m^3)
σ	liquid surface tension (N/m)

Subscripts

A	quantity measured in air
EQ	Equivalent quantity

C	critical value at the fluidelastic threshold
G	gas phase
GS	Superficial gas phase
H	quantity calculated by the homogeneous equilibrium model
L	liquid phase
LS	Superficial liquid phase
P	pitch quantity
RAD	quantity corresponding to radiation attenuation method of void fraction measurement
HEM	quantity corresponding to homogeneous equilibrium model for void fraction measurement

References

Axisa, F., Boheas, M.A., Villard, B., 1985. Vibration of tube bundles subjected to steam–water cross-flow: a comparative study of square and triangular arrays. Paper B1/2 in the Eighth International Conference on Structural Mechanics in Reactor Technology, Brussels, Belgium.

Chan, A.M.C., Banerjee, S., 1981. Design aspects of gamma densitometers for void fraction measurements in small scale two-phase flows. Nuclear Instruments and Methods 190, 135–148.

Chen, S.S., 1983. Instability mechanisms and stability criteria of a group of circular cylinders subjected to cross-flow, Part I: Theory; Part II: numerical results and discussions. ASME Journal of Vibration, Acoustics, Stress and Reliability in Design, 105, 51–58, 235–260.

Chen, S.S., 1984. Guidelines for the instability flow velocity of tube arrays in cross-flow. Journal of Sound and Vibration 93, 439–455.

Feenstra, P.A., Judd, R.L., Weaver, D.S., 1995. Fluidelastic instability in a tube array subjected to two-phase R-11 cross-flow. Journal of Fluids and Structures 9, 747–771.

Feenstra, P.A., Weaver, D.S., Judd, R.L., 2000a. Modelling two-phase flow-excited fluidelastic instability in tube arrays. In: Ziada, S., Staubli, T. (Eds.), Proceedings Flow-Induced Vibration, Lucerne, Switzerland. A.A. Balkema, The Netherlands, pp. 545–554.

Feenstra, P.A., Weaver, D.S., Judd, R.L., 2000b. An improved void fraction model for two-phase cross-flow through horizontal tube arrays. International Journal of Multiphase Flow 26, 1851–1873.

Grant, I.D.R., Murray, I., 1972. Pressure drop on the shell-side of a segmentally baffled shell-and-tube heat exchanger with vertical two-phase flow. Report NEL-560, National Engineering Lab.

Hirota, K., Nakamura, N., Mureithi, N.W., Kasahara, J., Kusakabe, T., Takamatsu, H., 1996. Dynamics of an inline tube array in steam–water flow. Part III: fluidelastic instability tests and comparison with theory. In: Pettigrew, M.J. (Ed.), Proceedings ASME PVP Conference, PVP Vol. 328, Montreal, pp. 123–134.

Judd, R.L., Dam, R., Weaver, D.S., 1992. A photo-optical technique for measuring flow-induced vibrations in cantilevered tube bundles. Experimental Thermal and Fluid Science 5, 747–754.

Li, M., Weaver, D.S., 1997. A fluidelastic instability model with an extension to full flexible multi-span tube arrays. In: Païdoussis, M.P. (Ed.), Proceedings of the ASME PVP Conference, Vol. II. Flow-Induced Vibration and Noise, Dallas.

Mann, W., Mayinger, F., 1995. Flow-induced vibration of tube bundles subjected to single and two-phase cross-flow. Proceedings of the Second International Conference on Multiphase Flow 4, Kyoto, Japan.

Nakamura, T., Hirota, K., Tomomatsu, K., Kasahara, J., Takamatsu, H., 1999. On positional effect of flexible tubes in a square array subjected to Freon two-phase flow. In: Pettigrew, M.J. (Ed.), Proceedings of the ASME PVP symposium, PVP-Vol. 389. Flow Induced Vibration, Boston, pp. 73–80.

Nakamura, T., Hirota, K., Tomomatsu, K., 2000. Some problems on the estimation of flow-induced vibration of a tube array subjected to two-phase flow. In: Ziada, S., Staubli, T. (Eds.), Proceedings Flow-Induced Vibration, Lucerne, Switzerland. A.A. Balkema, The Netherlands, pp. 537–544.

Nicklin, D.J., Wilkes, J.C., Davidson, J.F., 1962. Two-phase flow in vertical tubes. Transactions of the Institute of Chemical Engineers 40, 61–68.

Paidoussis, M.P., 1982. A Review of Flow Induced Vibrations in Reactors and Reactor Components. Nuclear Engineering and Design 74, 31–60.

Pettigrew, M.J., Taylor, C.E., 1994. Two-phase flow-induced vibration: an overview. ASME Journal of Pressure Vessel Technology 116, 233–253.

Pettigrew, M.J., Taylor, C.E., Kim, B.S., 1989a. Vibration of tube bundles in two-phase cross flow. Part 1—Hydrodynamic mass and damping. Journal of Pressure Vessel Technology 111, 466–477.

Pettigrew, M.J., Tromp, J.H., Taylor, C.E., Kim, B.S., 1989b. Vibration of tube bundles in two-phase cross-flow: Part 2—fluid-elastic instability. ASME Journal of Pressure Vessel Technology 111, 478–487.

Pettigrew, M.J., Taylor, C.E., Jong, J.H., Currie, I.G., 1995. Vibration of a tube bundle in two-phase freon cross-flow. ASME Journal of Pressure Vessel Technology 117, 321–329.

Taitel, Y., Bornea, D., Dukler, A.E., 1980. Modelling flow pattern transitions for steady, upward gas–liquid flow in vertical tubes. A.I.Ch.E. Journal 26, 345–354.

Ulbrich, R., Mewes, D., 1994. Vertical, upward gas–liquid two-phase flow across a tube bundle. International Journal of Multiphase Flow 20, 249–272.

Weaver, D.S., Yeung, H.C., 1983. Approach flow direction effects on the cross-flow induced vibrations of a square array of tubes. Journal of Sound and Vibration 87, 469–482.

Weaver, D.S., Abd-Rabbo, A., 1985. A flow visualization study of a square array of tubes in water cross-flow. ASME Journal of Fluids Engineering 107, 354–363.

Weaver, D.S., Fitzpatrick, J.A., 1988. A review of cross-flow induced vibrations in heat exchanger tube arrays. Journal of Fluids and Structures 2, 73–93.

Weaver, D.S., Ziada, S., Au-Yang, M.K., Chen, S.S., Paidoussis, M.P., Pettigrew, M.J., 2000. Flow-induced vibrations in power and process plant components—progress and prospects. ASME Journal of Pressure Vessel Technology 122, 339–348.

Whalley, P.B., 1987. Boiling, Condensation and Gas–Liquid Flow. Oxford University Press, New York.